New use for old drug: Local delivery of puerarin facilitates critical-size defect repair in rats by promoting angiogenesis and osteogenesis

Huijuan Cao [a,b,d,g,1], Lingli Li [a,c,1], Ling Li [a,d,g,1], Xiangbo Meng [a,d,g], Yanzhi Liu [a,e], Wenxiang Cheng [a,d,g], Peng Zhang [a,d,g], Yongbo Gao [c,**], Ling Qin [a,d,f,***], Xinluan Wang [a,b,d,g,*]

[a] Centre for Translational Medicine Research & Development, Shenzhen Institutes of Advanced Technology, Chinese Academy of Sciences, Shenzhen, PR China
[b] University of Chinese Academy of Sciences, Beijing, PR China
[c] Shenzhen Clinical Medical College of Guangzhou University of Chinese Medicine, Shenzhen, PR China
[d] Joint Laboratory of Chinese Academic of Science and Hong Kong for Biomaterials of the Chinese University of Hong Kong, PR China
[e] Guangdong Key Laboratory for Research and Development of Natural Drugs, Department of Pharmacology, Guangdong Medical University, Zhanjiang, PR, China
[f] Musculoskeletal Research Laboratory, Department of Orthopaedics & Traumatology, The Chinese University of Hong Kong, Hong Kong SAR, PR China
[g] Key Laboratory of Health Informatics, Chinese Academy of Sciences, Shenzhen, PR China

ARTICLE INFO

ABSTRACT

Objectives: Large bone defect repair is a challenging clinical problem due to limited self-repair ability. A well-designed bone filling product should possess the ability to induce tissue in-growth and facilitate neo-vascularization and new bone formation. Puerarin has been used in clinics for a long time, and recently it was found to be able to promote osteogenesis. This study aimed to investigate a puerarin-based drug/delivery combination implant for promoting large bone defect repair.
Methods: Puerarin was incorporated into the poly (lactic-co-glycolic acid)/β-calcium phosphate (PLGA/TCP, PT) to form a porous PLGA/TCP/Puerarin (PTP) composite scaffold by low-temperature rapid prototyping technology. Its structural and degradation were analyzed *in vitro*. Then we employed a rat calvarial critical size defect model to assess the potency of the PTP scaffold. MC3T3-E1 cells and EA. hy 926 cells were used to investigate the underlying mechanism.
Results: PTP scaffold inherited all advantages of PT scaffold in structural, mechanical, and biodegradation, meanwhile puerarin stably and continuously released from PTP scaffold and lasted for 5 months *in vitro*. At 8 weeks after implantation, the PTP scaffold triggered new bone formation in the macro-pores of the scaffold and inside the scaffold accompanied by the degrading materials. The underlying mechanism revealed that the PTP scaffold induced vascular infiltration and recruit repair cells through stimulating vascular endothelial growth factor (VEGF) and bone morphogenetic protein 2 (BMP-2) expressions to promote angiogenesis and osteogenesis.
Conclusion: Puerarin-enriched porous PTP scaffold was a promising local delivery system with sustained release of puerarin for facilitating defect repair through getting synergistic angiogenic and osteogenic effects.

 * Corresponding author. Shenzhen Institutes of Advanced Technology Chinese Academy of Sciences, 1068 Xueyuan Avenue, Shenzhen University Town, Shenzhen, Guangdong, China.
 ** Corresponding author. Longgang District Central Hospital, Affiliated to Guangzhou University of Chinese Medicine, 6082 Longgang Avenue, Shenzhen, Guangdong, China.
 *** Corresponding author. Department of Orthopaedics & Traumatology, The Chinese University of Hong Kong, Prince of Wales Hospital, 5/F Lui Che Woo Clinical Sciences Building, Shatin, N.T., Hong Kong SAR, China.
 E-mail addresses: gaoyongbo2020@163.com (Y. Gao), lingqin@cuhk.edu.hk (L. Qin), xl.wang@siat.ac.cn (X. Wang).
 [1] The authors contributed equally to this paper.

The Translational Potential of this Article: The PTP scaffold presents a potential drug/device combination medical implant for large bone defect repair, which also provides a new and innovative application for the "old drug" puerarin.

1. Introduction

Bone is a highly vascularized tissue, and insufficient bone vascularity results in a decrease in bone formation potential and reduction of bone mass [1]. Bone tissue possesses a natural regenerative capacity that is sufficient for the healing of small size damage. However, bone defects that exceed the critical size threshold will not heal unaided [2,3]. Bone defect repair is a complex process [4]. After the injury, the impaired bone region would undergo inflammation response first, and then recruit various reparative cells to reside and survive within the injured regions, then those cells secret endogenous growth factors/cytokines in favor of angiogenesis, bone regeneration, and remodeling activation [4,5]. Bone fracture repair is ordered in a sequence-dependent manner and seemingly relates to vascular patterns [6]. Fast vascularization results in a rapid response to biophysical stimuli and biochemical signaling, ultimately achieving sufficient bone repair [7]. Negative effects on the vascular system might be the mechanism whereby many other risk factors delay or impair bone healing [6]. Thus, an ideal medical implant should possess the ability to conduct implant and host-tissue receptivity at the beginning of healing, but also could regulate vascular patterns for promoting bone regeneration *in suit* by mobilizing the recipient's cells. Controlled delivery of endogenous growth factors such as vascular endothelial growth factor (VEGF) and bone morphogenetic protein 2 (BMP-2) could mobilize reparative cells to enhance revascularization and bone regeneration [8–10]. However, the safety and cost-effectiveness of these biological factors limited their use [9,11].

Our previous work has established an excellent porous poly (lactic-co-glycolic acid) (PLGA)/beta-tricalcium phosphate (β-TCP) (PLGA/TCP, PT) scaffold by low-temperature rapid prototyping (LT-RP) technology to deliver bioactive substances, such as icariin, icaritin, salvianolic acid, and magnesium particles, to promote new bone formation in challenging healing bone defects [12–16]. However, the addition of bioactive substances may result in new intended uses with unfavorable factors during bench-to-bedside translation, causing safety and efficacy issues [17]. In China, drug/device combination products with main effects as medical devices shall be regulated as Class III medical devices, and drugs in combination products should have a drug registration certificate issued by National Medical Products Administration (NMPA) [17].

Puerarin, 4H-1-benzopyran-4-one,8-b-D-glucopyranosyl-7-hydroxy-3-(4-hydroxy-phenyl) C12H20C9, is the major active ingredient isolated from the root of a wild leguminous creeper, *Pueraria lobata (Willd.) Ohwi*, which has been widely used as a food supplement or medicine in China [18,19], and puerarin is easy to obtain and purify [20]. There have been injection, tablet, and capsule forms of puerarin available for the treatment of cardiovascular and cerebrovascular diseases clinically [20]. Recent studies suggested that puerarin could prevent bone loss by inhibiting osteoclastic bone absorption and promoting osteoblastic bone formation in ovariectomized mice [18,21–23]. A previous study also demonstrated that puerarin combined with autogenous graft material which was filled into rat calvarial bone defect region could enhance the efficacy of autologous bone graft [24]. Meanwhile, when puerarin solution mixed with collagen matrix implantation could improve new bone formation in rabbit calvarial bone defects [25]. Therefore, puerarin might be the long-sought-after safe and ideal medicine combing with PT scaffold as a drug/device combination implant for promoting large defect bone repair.

In this study, puerarin was incorporated into PT to fabricate a puerarin-enriched composites scaffold (PLGA/TCP/Puerarin, PTP) using LT-RP technology [12]. We employed a rat calvarial critical-size defect model to assess the potency of the PTP scaffold. The imaging techniques and histological assessments were used for quantitative evaluation of newly formed blood vessels and bone tissue. MC3T3-E1 cells and EA. hy 926 cells were used to investigate the underlying mechanism.

2. Materials and methods

2.1. Chemicals and reagents

Puerarin (>99.98%, Fig.S1) was provided by Chengdu Herbpurify Corporation (Lot.20,150,301, Chengdu, China); PLGA (lactide to glycolide mole ratio = 75:25; weight average molecular weights [Mw] = 115000, number average molecular weight [Mn] = 10600, and poly dispersity [Mw/Mn] = 1.2; average viscosity = 1.70 ± 0.02 dl g-1) from the Institute of Biomaterials of Shandong (Shandong, China); Amorphous TCP ceramic powders with 50 μm diameter from Beijing Modern Orient Precise Chemical Articles Co., Ltd (Beijing, China); 1,4-dioxane from Aladdin (Shanghai, China); Dimethyl formamide (DMF) from J&K Scientific Corporation (Beijing, China); Minimum essential medium eagle-alpha modification (α-MEM), Dulbecco's modified eagle medium (DMEM), fetal bovine serum (FBS), penicillin-streptomycin (PS) and trypsin from HyClone Laboratories Inc(Logan, UT,USA); Alizarin red S, β-glycerol phosphate and ascorbic acid from Sigma–Aldrich (St. Louis, MO, USA); Cell counting kit-8 (CCK-8) from DOJINDO Lab (Tokyo, Japan); Matrigel® Matrix (354234) from Corning Incorporated (Corning, NY, USA). Polyvinylidene fluoride (PVDF) membrane from Bio-Rad Laboratories (Hercules, CA, USA); Enhanced chemiluminescence detection kit from Multi Sciences Biotech Co. Ltd (Hangzhou, China); Anti-hypoxic induction factor-1 alpha (HIF-1α) (MAB5382) from Millipore (USA), anti-vascular endothelial growth factor A (VEGF-A) (ab28775), anti-bone morphogenetic protein 2 (BMP-2) (ab6285), anti- β-actin (ab8227) (ab8245), goat anti-rabbit lgG H&L (HRP) (ab6721), goat anti-mouse lgG H&L (HRP) (ab6789), mouse and rabbit specific HRP/DAB (ABC) detection IHC Kit (ab64264) from Abcam (Cambridge, MA, USA). Tartrate-resistant acid phosphatase (TRAP) dye from Joytech Bio Co., Ltd (Zhejiang, China).

2.2. Preparation and fabrication of puerarin-enriched porous composite scaffolds

PTP scaffolds were prepared in a low-temperature 3D printing machine (CLRF-2000-II, Tsinghua University, Beijing, China) according to a predesigned 3D structure model and previously established fabrication protocol [13]. PLGA was dissolved in 1,4-dioxane to form a 10% (w/v) homogeneous solution and then mixed with TCP powder with a particle size of approximately 300 meshes. The mass ratio of PLGA: TCP was 4:1 (w/w) as previously used [13,26]. The mixture was stirred with a magnetic stirrer to form a uniform liquid paste. Puerarin was dissolved in DMF at the concentration of 1 g/ml, and different volume of puerarin solution was added to the paste to form three doses of PTP scaffolds, with 0.25%, 0.5%, or 1% of puerarin (w/w). The paste was squeezed out layer-by-layer in a computer-driven nozzle at −30 °C to form a homogenous cubic porous scaffold with a volume of $20 \times 20 \times 20$ mm^3. Lyophilization was performed to remove 1,4-dioxane and DMF. A pure PLGA/TCP (PT) scaffold was used as comparison.

2.3. Scaffold characterization assay

2.3.1. Morphological observation and porosity measurement

The morphology and porosity of the scaffold were observed and measured according to an established protocol [14]. The macrostructure

and connectivity of the scaffold were visualized by micro-CT (Skyscan 1176, Bruker, Belgium) with a spatial resolution of 18 μm, at 45 kV, 500 μA, with 2 average frames at every 0.5° angle step. Reconstructed data were further evaluated by CT-Analyzer by controlling the minimum grey threshold value set at 30 HU (Hounsfield unit) up to a maximum of 255 HU. The surface morphology was observed by Scanning Electron Microscope with Energy Dispersive Spectrometer (SEM-EDS) (S-4800, Hitachi, Tokyo, Japan). Before performing SEM, the surface of the scaffold was coated with a thin layer of gold to provide electrical conductivity. The average pore size of the scaffold section surface was determined by the SEM photographs. The porosity was determined by the ethanol replacement method. The samples were cut into cubes (10 × 10 × 10 mm^3), and the volume and weight were recorded as V and W1. Next, the scaffold was immersed in alcohol. Then the scaffold had been taken out until there was no bubbling, and the weight was recorded as W2. The porosity was calculated following the equation (W2–W1)/density of alcohol/V.

2.3.2. Mechanical properties

The scaffolds were prepared by a published method yet with some modifications [14], then the mechanical properties of the scaffolds were tested and measured by a static and dynamic material testing machine (Instron-E3000, Norwood, MA, USA) with a load of 250 N and speed of 1 mm/min, 6 samples in each group were tested and the load–displacement curves were obtained. The load–displacement curves were used to calculate Young's modulus and compressive strength of the scaffolds based on ISO 844:2004 (www.iso.org).

2.3.3. Degradation

The scaffolds and their degradation solution were prepared by a published method with modification [27]. In brief, scaffolds were cut into a cube (12.5 × 12.5 × 10 mm^3). After sterilization under UV light, they were put into glass bottles. Then the scaffolds were immersed in phosphate-buffered saline (PBS) solution (pH = 7.4) according to a mass volume ratio of 1 g: 15 ml based on GB/T 16886.13–2001 and GB/T16886.12–2001. The scaffolds were shaken in a thermostatic water bath bed (the speed was 70 rpm, and the temperature was 37 °C) and the degradation solution was collected twice a week until complete degradation. The released Ca^{2+} ions in the degradation solution were determined by inductively coupled plasma mass spectrometry (ICP, Agilent 710, California, USA). The content of puerarin in the releasing solution was determined by high-performance liquid chromatography (HPLC, LC-20A HPLC system, Shimazu Corp., Kyoto, Japan) [13]. The preparation of standard and sample solutions, as well as the detailed HPLC procedures, were in Supporting Materials and Methods S1.

2.4. Biosafety and bioactivity study in vitro

2.4.1. Cell culture

Pre-osteoblastic cell line MC3T3-E1 (Subclone 14, CRL-2594) was purchased from ATCC (American Type Culture Collection, Manassas, VA, USA) and maintained in a growth medium (α-MEM with 10% FBS and 1% PS). The human umbilical vein cell line EA. hy 926 (CRL-2922, ATCC, USA) was provided by the Chinese University of Hong Kong. The EA. hy 926 cells were cultured in DMEM containing 10% FBS and 1% PS.

2.4.2. Degradation medium preparation

Experimental scaffolds in each group were dipped into α-MEM with 1% PS, respectively, and the mass of scaffold to α-MEM volume ratio is 1 g:10 ml according to the guideline "biological evaluation of medical devices-Part 12: Sample preparation and reference materials" (ISO 10993–12:2012). The differentiation medium was prepared according to previously established methods [28]. Briefly, after degradation for 2 days at 37 °C, the degradation medium was collected. Some degradation medium was diluted 10 folds by osteogenic medium (the growth medium containing 10 mM β-glycerol phosphate and 50 μg/mL ascorbic acid) for the following *in vitro* osteogenic activity assay, and some were diluted 10 folds by free-serum DMEM for tuber formation assay.

2.4.3. Biosafety assay in vitro

EA.hy 926 cells and MC3T3-E1 cells were seeded at 5000 cells/well in 96-well plates. After 24 h of incubation, the cells were treated with the diluted degradation medium. After the cells were incubated for 24, 48, and 72 h, respectively, then replaced the 100 μl free–serum medium (content 10% CCK-8) and incubated the sample at 37 °C for 30 min. Finally, the optical density (OD) value was measured at 490 nm in a Multiskan Sky microplate reader (Thermo Scientific, USA). The relative survival rate (RSR; %) was calculated using the following equation: RSR = (OD$_{scaffold\ degradation\ medium}$/OD $_{normal\ medium}$) × 100% [12].

2.4.4. Alizarin red S staining

MC3T3-E1 cells were plated at a density of 3×10^4 cells/well in 12-well tissue culture plates in the growth medium for reaching confluence, then incubated in an osteogenic differentiation medium containing degradation ingredients. After 18 days, the differentiation medium was removed, and cells were fixed with 3.7% (vol/vol) formaldehyde in PBS for 30 min followed by being rinsed with sterile water. 1% Alizarin red S staining working solution (pH = 2.63) was added to the fixed cells and incubated for 30 min. Then the cells were washed with sterile water three times to remove the staining solution. The calcium deposition was dissolved by 10% cetylpyridinium chloride monohydrate at room temperature for 30 min, then the OD value of the dissolved solution was detected at a wavelength of 562 nm.

2.4.5. Tube formation assay

Tube formation assay was performed according to Corning® Matrigel Matrix instruction. In brief, 0.15 ml of chilled Corning Matrigel Matrix (10 mg/ml) were added to 48 well culture plates on ice. The plate was then incubated at 37 °C for at least 30 min to initiate gelling. EA. hy 926 cells (12×10^4 cells) were then seeded in each well and incubated for 2 h. After incubation, the cells were treated with the scaffold degradation medium which was diluted for 10 folds in a serum-free medium. After 12 h of incubation, the well was photographed using the inverted phase-contrast microscope. The number of Junctions and total length were quantified using a plug-in, Angiogenesis Analyzer in NIH Image J software (National Institutes of Mental Health, Bethesda, MD, USA).

2.5. Bone regeneration study in vivo

2.5.1. Animal model and scaffold implantation

Thirty 12-week-female SD rats were provided by Guangdong Medical Laboratory Animal Center (Guangzhou, China) and maintained in a common facility at Shenzhen Institutes of Advanced Technology (Shenzhen, China). The animal experimental protocol was approved by the Research Ethics Committee of Shenzhen Institutes of Advanced Technology (SIAT-IRB-170814-YGS-ZP-A0370). The calvarial bone defect surgery in rats was performed to make critical size bone defects based on established protocol [29]. The animals were anesthetized with 2.5% isoflurane using a respiratory anesthesia device (ASA 1464, England, UK). A sagittal incision, 1.5–2 cm, was made on the scalp of each rat, and the calvaria was exposed by blunt dissection. Two 5 mm diameter and 1 mm thickness critical-sized defects were generated using a round carbide bur on the parietal bone, on both sides of the sagittal suture. The defects were randomly allocated into the following study groups: (1) empty defect as negative control group (n = 10); (2) PT scaffold implantation as positive control group (n = 10); (3) 0.5% PTP scaffold implantation as experimental group (n = 10). The shape and size of the cylindrical scaffold discs were adjusted to fit into the defects with a diameter of 5 mm and a thickness of 1 mm and implanted into the rats. The incision was closed in layers using sterile silk sutures.

2.5.2. Magnetic resonance imaging (MRI)

At 3, 5, and 7 weeks after implantation, the anesthetized SD rats were placed in a lateral position with limbs fixed by adhesive tape. Before the dynamic magnetic resonance imaging scan (3.0TMRI, uMR790, United-imaging, China), a gradient-echo sequence (TR = 7.12 ms; TE = 3.03 ms; section thickness = 0.5 mm) was employed. After 30 baseline images were acquired, 0.2 ml contrast agent gadopentetate dimeglumine (0.8 mmol/kg body weight) (Med Chem Express, USA) was injected into the tail vein of the rats. After that, 1 ml saline was administrated to flush the tail vein of the rats. The total thickness of the MRI scanning was analyzed to calculate the mean value describing the blood flow in defect areas [16].

2.5.3. Neovascularization analysis (microfil perfusion)

Eight weeks after implantation, the anesthetized SD rats were placed in a lateral position with limbs fixed by adhesive tape. The neck of the rat was opened, and the carotid aorta and carotid vein were separated. We continuously flushed the blood circulation through the carotid aorta until the vein outflow was clear. Afterward, 10 ml pre-warmed 10% formalin was injected into the carotid aorta of the anesthetized rats to clear and fix the vessels. 10 ml liquid compound of MV-Diluent, MV-117 Orange, and MV Curing Agent (MV-Diluent: MV-117 Orange: MV Curing Agent = 47.5: 38: 4.5) (Flow Tech Inc, USA) was slowly injected into the carotid artery at the moment when they were mixed. After that, the rats were sacrificed and stored in a 4 °C freezer for 24 h to ensure the microfilm mixture was clotted completely. Finally, the calvarial bone was collected and fixed in 10% formalin for 3 days, then the fixed samples were prepared for decalcification in 10% ethylene diamine tetra-acetic acid (EDTA, pH = 7.4) solution. As recommended by the relevant guidelines [14]. Micro-CT (Skyscan 1176, Bruker, Belgium) with a spatial resolution of 9 μm was used to evaluate the vessels in the calvarial bone samples under Al 0.5 filter. The 1.6 version of NR econ software and CT-Analyzer were used to reconstruct and analyze the 3D angiographic architecture of the samples by controlling the threshold of more than 60 HU [30].

2.5.4. Dual-energy X-ray and micro-CT analysis

Eight weeks after implantation, the calvarial bone defects of rats were scanned and analyzed by a dual-energy X-ray (DXA) body composition analysis system. A 5.0 mm-round centered area within defect regions was selected to calculate the bone mineral density (BMD, g/cm^2). The animals were sacrificed by intraperitoneal injecting 90–120 mg/kg of sodium pentobarbital, and the calvarial bone was collected and fixed in 10% formalin for one week [29]. Then micro-CT with a spatial resolution of 9 μm was used to scan the calvaria bone of the rats under the Al 0.5 filter which is defined by a threshold of more than 60 HU. A region of interest (ROI) of 4.5 mm diameter and 1.0 mm thickness was selected and reconstructed by CT-analyzer at the center of the calvaria bone defect to measure the ratio of bone volume (BV/TV, %).

2.5.5. Histological evaluation

Eight weeks after implantation, the animals were sacrificed and the calvarial bone was collected and fixed in 10% formalin for 3 days. Then the fixed samples were decalcified into 10% EDTA (pH = 7.4) solution. The status of decalcification and concentration were monitored during decalcification. After decalcification, the calvarial bone was embedded in paraffin and the middle region was cut into serial 5-μm-thick sections. Sections were stained with Hematoxylin and Eosin (H&E) and Safranin O/Fast green for routine histology. Meanwhile, sections were stained with TRAP dye for the identification of osteoclasts. The H&E stained sections were used to score and evaluate the new bone ingrowth within the pores of the scaffolds according to published reports [31,32]. Bone growth within scaffold pores and polymer degradation and bone formation within the defect were evaluated using revised criteria (Table S2). These grey-white and few cells zone were identified as residual scaffold according to the published papers [30,33], which could clearly be distinguished from surrounding tissues.

To verify the effects of PT and PTP scaffold on HIF-1α, VEGF, BMP-2 expressions, and type H vessels formation within implantation regions, HIF-1α was stained by immunohistochemistry with a 1/100 dilution of HIF-1α antibody, VEGF and BMP-2 were stained by immunohistochemistry with 1/200 dilution of VEGF and BMP-2 antibody, respectively. And then the images were observed by Leica DMi8 microscope (Leica, Wetzlar, Germany). The staining was quantified by Image-Pro Plus software (Version6.0, Media Cybernetics, American).

2.6. Statistical analysis

Data of scaffold degradation analysis, bioactivity analysis *in vitro*, quantitative analysis of new bone formation from micro-CT, histological analysis, and blood perfusion analysis of DCE-MRI *in vivo*, new vessel formation analysis of CT-based microfil in *ex-vivo* all were expressed as Mean ± SD, and one-way ANOVA followed by *post-hoc* Bonferroni's multiple comparisons was performed to assess statistical significance between two groups. Initiated mechanical properties and physical structure properties of scaffolds were expressed as Mean ± SD, and a t-test was performed to assess statistical significance. Significance was set at $p < 0.05$. Statistical analysis was performed with Graphpad Prism 6 software (Graphpad Software Inc, San Diego, CA, USA).

3. Results

3.1. PTP scaffold fabrication and characterization

All scaffolds were fabricated uniformly at $20 \times 20 \times 20$ mm^3 with regular macropores. PTP scaffolds matrix was white. PTP scaffolds with different ratios of puerarin had homogeneous porous structures. The structure of the 0.5% PTP scaffold observed by micro-CT and SEM were showed in Fig. 1. The reconstructed micro-CT images showed that the PTP scaffold had an interconnected structure both horizontally and vertically, and the pores were highly interconnected. Pore connectivity of the scaffolds was close to 100%. The porosity of PTP scaffolds was 66.59 ± 3.35% (Table 1), and that of PT scaffolds was 62.03 ± 1.05%. The pore size of the PTP scaffolds was 465 ± 11.89 μm, and that of the PT scaffolds was 484 ± 10.06 μm. There was no significant difference in the porosity, pore size, and pore connectivity between the scaffolds with or without puerarin. However, puerarin incorporation could enhance the mechanical strength of the porous scaffold. The compressive strength of the PTP scaffold was 1.08 ± 0.05 MPa, which was significantly higher ($p < 0.05$) than that of the PT scaffold (0.95 ± 0.04 MPa). The Young's modulus of the PTP scaffold was 24.70 ± 4.90 MPa, showing no significant difference when compared to that of PT scaffolds (21.72 ± 1.89 MPa).

3.2. PTP scaffold degradation and biosafety in vitro

Puerarin loading efficacy in PTP scaffolds was determined by HPLC. Over 85% of puerarin was loaded in PTP scaffolds during fabrication (Table.S1). During the degradation process, PTP scaffolds showed more stability and maintained their porous structure for at least 10 weeks, the macro-structure deformation occurred until 73 days after degradation and deformed to powder completely at 196 days (Fig. S2A&B). The pH value of the degraded medium maintained at 7.0–7.5 before 10 weeks, then the pH value declined and reached the lowest value (pH = 4.5) at 150 days (Fig. 2A). As expected, the Ca^{2+} ions concentration increased sharply after 123 days after degradation (Fig. 2B), while the pH value of the degradation solution ascended gradually. The pH value changed and Ca^{2+} ions released in the PT and PTP scaffolds maintained the same trend and level. The content of puerarin in the PTP scaffold did not affect the pH value change and Ca^{2+} ions release. The release rate of puerarin was independent of puerarin ratios in PTP scaffolds (Fig. 2C). The release rate increased at 49 days and then slowed down at 108 days after degradation. The cumulative released puerarin content of 0.25%, 0.5%, 1% PTP scaffolds were 70.76%, 79.59% and 75.57%, respectively.
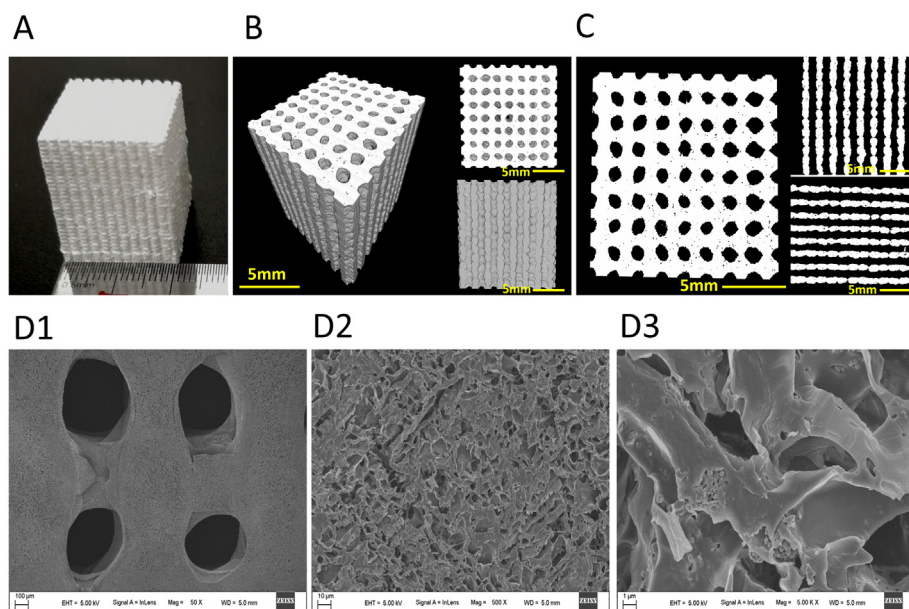
Fig. 1. Scaffold characterization. A: Photo of 0.5% PTP scaffold with the size of $2 \times 2 \times 2$ cm^3. B–C: Morphology observation of PTP by micro-CT. B: Reconstructed 3D images of PTP scaffold, transverse section 3D structure, and vertical section 3D structure (bar = 5 mm). C: 2D images of PTP scaffold, transverse section 2D structure, and vertical section 2D structure (bar = 5 mm). D: Morphology observation of PTP by SEM. D1: Transverse section, $50 \times$ (bar = 100 μm); D2: Micro-structure of the pore surface of PTP scaffold, $500 \times$ (bar = 10 μm); D3: Nano-structure of the pore surface of PTP scaffold, $500K \times$ (bar = 1 μm).

Table 1

Macro pore size, porosity, connectivity, and mechanical properties of scaffolds. The PTP scaffold contained 0.5% wt of puerarin.

	[a]Pore size (μm)	[b]Porosity (%)	[c]Pore connectivity (%)	Young's modulus (MPa)	Compressive strength (MPa)
PT	484 ± 10.06	62.03 ± 1.05	100	21.72 ± 1.89	0.95 ± 0.04
PTP	465 ± 11.89	66.59 ± 3.35	100	24.70 ± 4.90	1.08 ± 0.05[d]

[a] The macropore size of the porous scaffold was evaluated by SEM.

[b] The porosity of the porous scaffolds was determined by ethanol replacement and calculated according to the equation.

[c] The connectivity of the pore structure of the porous scaffold was determined by micro-CT.

[d] $p < 0.05$.

Meanwhile, the biosafety of the PTP scaffold degradation medium was analyzed. The concentration of puerarin in the degradation medium was measured by HLPC. The content of puerarin was 23.806 μM, 53.044 μM and 249.014 μM in 0.25%, 0.5% and 1%PTP degradation medium, respectively (Fig.S3A). Then, the degradation medium was diluted for 6 or 10 folds using a growth medium for the following *in vitro* studies. The degradation medium of 0.5% PTP scaffolds exhibited good biocompatibility, while the RSR in the 1% PTP group was lower than the PT group at 24 and 72 h (Fig.S3). Especially, the degradation medium of the 0.5% PTP scaffold significantly promoted MC3T3-E1 cells proliferation ($p <$ 0.01) when compared to that of the PT scaffold (Fig. 2D1). Although the degradation medium of 0.5% PTP scaffold did not affect the proliferation of EA. hy 926 cells (Fig. 2D2), when the cells were seeded on the scaffold and cultured for 72 h, they preferred to attach on the 0.5% PTP scaffold rather than on the PT scaffold (Fig.S4).

3.3. PTP scaffold showed better bioactivity in vitro

The bioactivities of the degradation medium of PTP scaffold on promoting bone formation and vessel formation *in vitro* were detected in this study. In terms of osteogenesis *in vitro*, the degradation medium of all scaffolds could accelerate calcium nodules formation of MC3T3-E1 cells after osteogenic induction for 18 days, especially 0.5% PTP group, which showed a significant difference from the PT group (Fig. 3A and Fig.S5).

Consistently, ALP activity also increased and reached its peak value on day 12 and declined on day 15 after induction, and the 0.5% PTP group showed a significant difference on day 12, but 0.25% and 1% PTP groups did not significantly up-graduate ALP activity when compared to PT group (Fig.S5). As to tube formation of EA. hy 926 cells on the Matrigel, there were many tube-like structures observed when the cells were exposed to the degradation medium of those PTP scaffolds for 12 h, while that of the 1% PTP group showed a suppressing effect on tube formation of EA. hy 926 cells (Fig. S6). The negative effect of the 1% PTP group on MC3T3-E1 cell and EA. hy 926 cells might be related to the high puerarin concentration in the degradation medium.

Although the tube formation in the 0.5% PTP group did not show a difference when compared to that of the PT group (Fig. 3B). However, when the EA. hy 926 cells were treated with the conditioned medium of MC3T3-E1 cells which were cultured by degradation medium of 0.5% PTP scaffolds for 2 days, there were more tube-like formations in the PTP group than PT group (Fig. 3C). Consistently, we further found that the MC3T3-E1 cells exposed to PTP degradation medium would up-gradate VEGF protein level at 3 days and BMP-2 level at 9 days than the normal and control groups, respectively, but showed no difference between PT and PTP groups (Fig. 3D). Collectivly, based on the better biosafety and bioactivity of the 0.5% PTP scaffold than that of 0.25% and 1% PTP scaffolds, we chose the 0.5% PTP scaffold as the PTP scaffold presenter in the following experiments for evaluating the efficacy *in vivo*.

3.4. Puerarin-enriched scaffold promoted new bone regeneration

The 3D reconstruction images of Micro-CT in Fig. 4A showed the new bone formation within the calvarial defect at 8 weeks post-implantation. The quantitative analysis of micro-CT demonstrated a marked difference between groups with and without scaffold implantation. PT scaffold and PTP scaffold could significantly improve new bone formation than that of the control group. Higher bone volume ratio (BV/TV, %) within the calvarial bone defect was found in the PTP group (10.89 ± 5.38%) ($p =$ 0.021) and PT group (10.55 ± 4.32%) as compared with the control group (3.28 ± 2.08%) (Fig. 4A), and without significant statistical differences between PT scaffold and PTP scaffold. Moreover, the PTP scaffold could significantly enhance bone mineral density (BMD, g/cm^2) of newly formed bone tissue compared with the PT scaffold ($p = 0.039$). The H&E staining showed that the scaffold implantation can promote orthotopic osteogenesis along the scaffold struts and within pores,
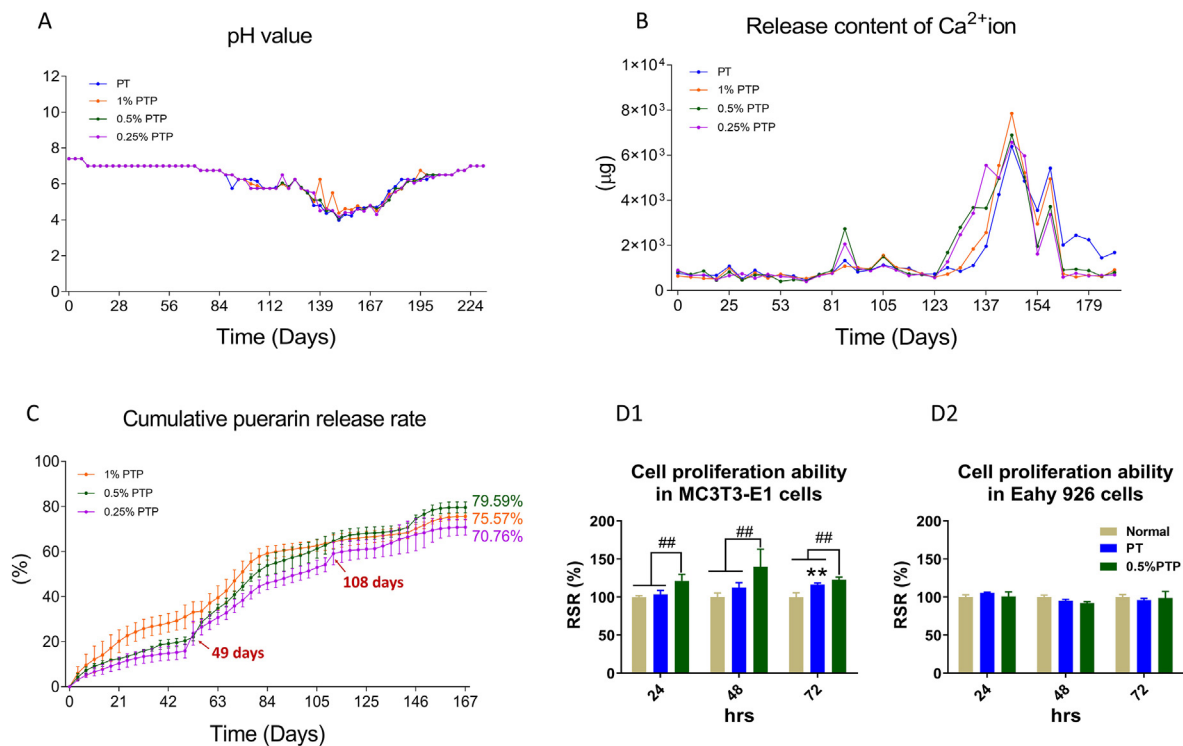
Fig. 2. Scaffold degradation and biosafety analysis. A–C: Ingredients releasing from a scaffold during degradation, n = 3. The pH value (A), the concentration of Ca^{2+} ion (B), and the cumulative puerarin releasing (C) in the medium during the degradation process. D: Biosafety analysis of degradation medium. Effect of degradation medium of 0.5% PTP and PT scaffolds on the toxicity of MC3T3-E1 (D1) and EA. hy 926 cells (D2). RSR (%): The relative survival rate. n = 6, **$p < 0.001$, when compared between the Normal group and PT group; ##$p < 0.01$, when compared to the PTP groups.

especially in the PTP group, while the control group only formed new bone at the edge of the calvarial defect (Fig. 4B1). The quantitative data of newly formed bone within the defect region showed no difference between PT and PTP groups (Fig. 4B2, Fig.S8). In addition, the area ratio of residual material in the implantation regions was less in the PTP group compared to the PT group ($p = 0.012$) (Fig. 4B3), suggesting that the PTP scaffold had a faster degradation rate than PT *in vivo*. The corresponding histological score results showed that the PTP group got a significantly higher score on polymer degradation ($p = 0.0005$) but demonstrated no significant difference in the scores of bone growth within scaffold pores ($p = 0.108$) and bone contact at the interface ($p = 0.382$) between PTP group and PT group (Fig.S7). Besides the newly formed bone and scaffold remaining in the defect region, we also observed lots of unmineralized tissues (Fig. 4C). The results of Safranin O/Fast green staining showed those tissues were unmineralized cartilage, and histomorphometry results revealed the unmineralized cartilage tissue increased by nearly 4 folds in the PTP group than that of the PT group ($p = 0.009$) (Fig. 4D). At the same time, there more activated tartrate-resistant acid phosphatase positive (TRAP+) cells were found in the regenerated tissue in the PTP group when compared to the PT group ($p = 0.008$) (Fig. 4E), this suggested that the remodeling program had been started as TRAP + cells fusing to be osteoclasts. No inflammation was found in the surgery area in all groups throughout the animal experiment.

3.5. Puerarin-enriched scaffold promoted neovascularization

The representative dynamic contrast-enhanced magnetic resonance imaging (DCE-MRI) signal and the 3D images of the neovascularization based on micro-CT in calvarial bone were shown in Fig. 5. The average information object definition (IOD) of MRI images in the PTP group was gradually increased from 3 weeks to 7 weeks post-surgery, and significantly higher than that in the PT group at 7 weeks (Fig. 5A). The vascular signal of the PT group had a slight decrease at 7 weeks (14.5% reduction)

compared with 5 weeks. Micro-CT-based angiography analysis was conducted to observe the newly formed vessels in the defect regions. Analysis of micro-CT-based angiography showed more newly formed vessels and more vascular numbers in the defects implanted with PTP scaffolds compared with PT scaffolds at 8 weeks post-surgery (Fig. 5B). The histology staining also showed more vessels after perfusion with microfils (Fig.S7). And PTP scaffold can significantly improve newly formed vascular volume than that of the control group ($p = 0.033$). The average vessel volume of the PTP group at 8 weeks was 0.48 ± 0.26 mm^3, and the average vessel volume of the PT group and Control group at 8 weeks were 0.16 ± 0.05 mm^3 and 0.005 ± 0.007 mm^3, respectively. The vessel number (1/mm) was increased in the PTP group (0.18 ± 0.13) and PT group (0.11 ± 0.02) compared with the Control group (0.003 ± 0.005). Meanwhile, we found that PTP scaffold could promote angiogenesis either small size (<100 μm), medium-sized (100–200 μm), or large-sized (>200 μm) within defect regions, while PT scaffold only promoted the formation of blood vessels less than 200 μm in diameter. And PTP group had a significant increase in small-sized (<100 μm) vessels compared with the Control group ($p = 0.0384$) within the calvarial bone defect (Fig. 5B).

3.6. Puerarin-enriched scaffold up-regulated VEGF and BMP2 levels

To further characterize osteogenesis and angiogenesis, immunohistochemical analyses of HIF-1α, VEGF, and BMP-2 were conducted (Fig. 6). In the Control group, there was no obvious positive staining for HIF-1α and VEGF within the defect region, which was more apparent in the PTP group. Significantly higher expression of HIF-1α was detected in the PTP groups compared with the PT group ($p = 0.004$) and the Control group ($p = 0.002$) (Fig. 6A&B). Correspondingly, the VEGF expression in the PTP group was higher than in the PT group ($p = 0.002$) and the Control group ($p = 0.001$) (Fig. 6B). Moreover, the PTP group also could significantly increase BMP-2 expression more than the Control group (p
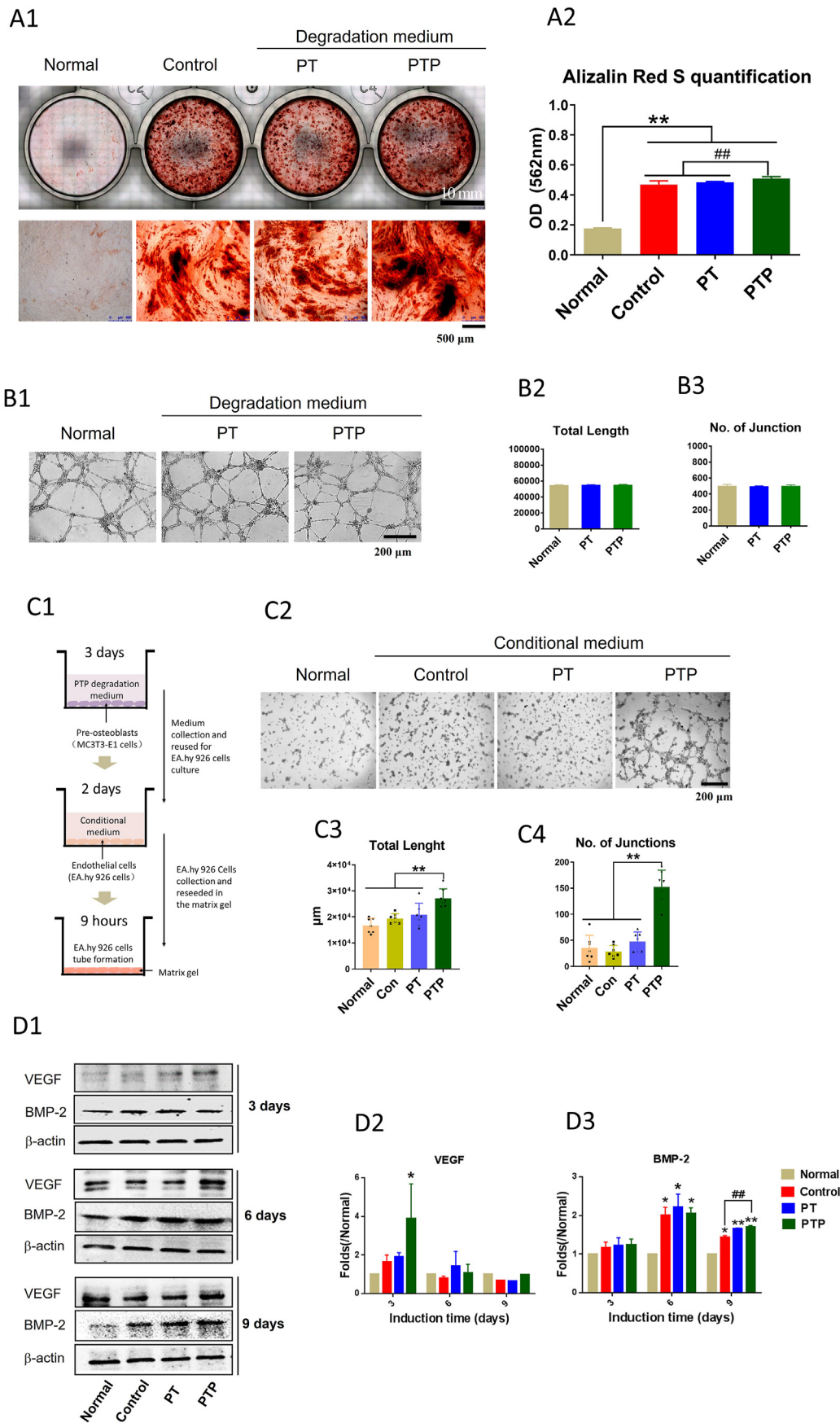
Fig. 3. *In vitro* osteogenic and angiogenic activities analysis. A: Calcium nodules formation of MC3T3-E1 cells cultured by osteogenic medium with degradation ingredients of 0.5% PTP scaffolds for 18 days. Alizarin Red S staining images (A1), above bar = 10 mm and below bar = 500 μm; and quantification assay of the calcium nodules (A2), n = 6. **$p < 0.01$, when compared to the Normal group; ##$p < 0.01$, when compared between PT (or Control) and PTP groups. B: The EA. hy 926 cells were treated with a degradation medium of 0.5% PTP scaffold on the Matrigel for 9 h. Tube-like structures of EA. hy 926 cells on the Matrigel (B1), bar = 200 μm. Tube formed *in vitro* quantitative data of total length (B2) and several junctions (B3) by image J software, n = 10. C: The conditioned medium was collected from MC3T3-E1 cells which had osteoblastic induced for 3 days, the EA. hy 926 cells were treated with condition medium for 2 days, then translated these cells on the Matrigel for other 9 h. The flow chart (C1). Tube-like structures of EA. hy 926 cells on the Matrigel (C2), bar = 200 μm. Tube formed *in vitro* quantitative data of total length (C3) and several junctions (C4) by image J software, n = 6. **$p < 0.01$. D: MC3T3-E1 cells were cultured in an osteogenic medium with degradation ingredients of PTP scaffold for 3, 6, and 9 days, and BMP-2 and VEGF-A protein levels were detected. Representative western blots of total BMP-2 and VEGF-A after induction in MC3T3-E1 cells (D1). Quantification of protein levels of VEGF (D2) and BMP-2 (D3) using β-actin as a reference, n=3. *$p < 0.05$, **$p < 0.01$, when compared to the Normal group; ##$p < 0.01$, when compared between Control and PTP groups.
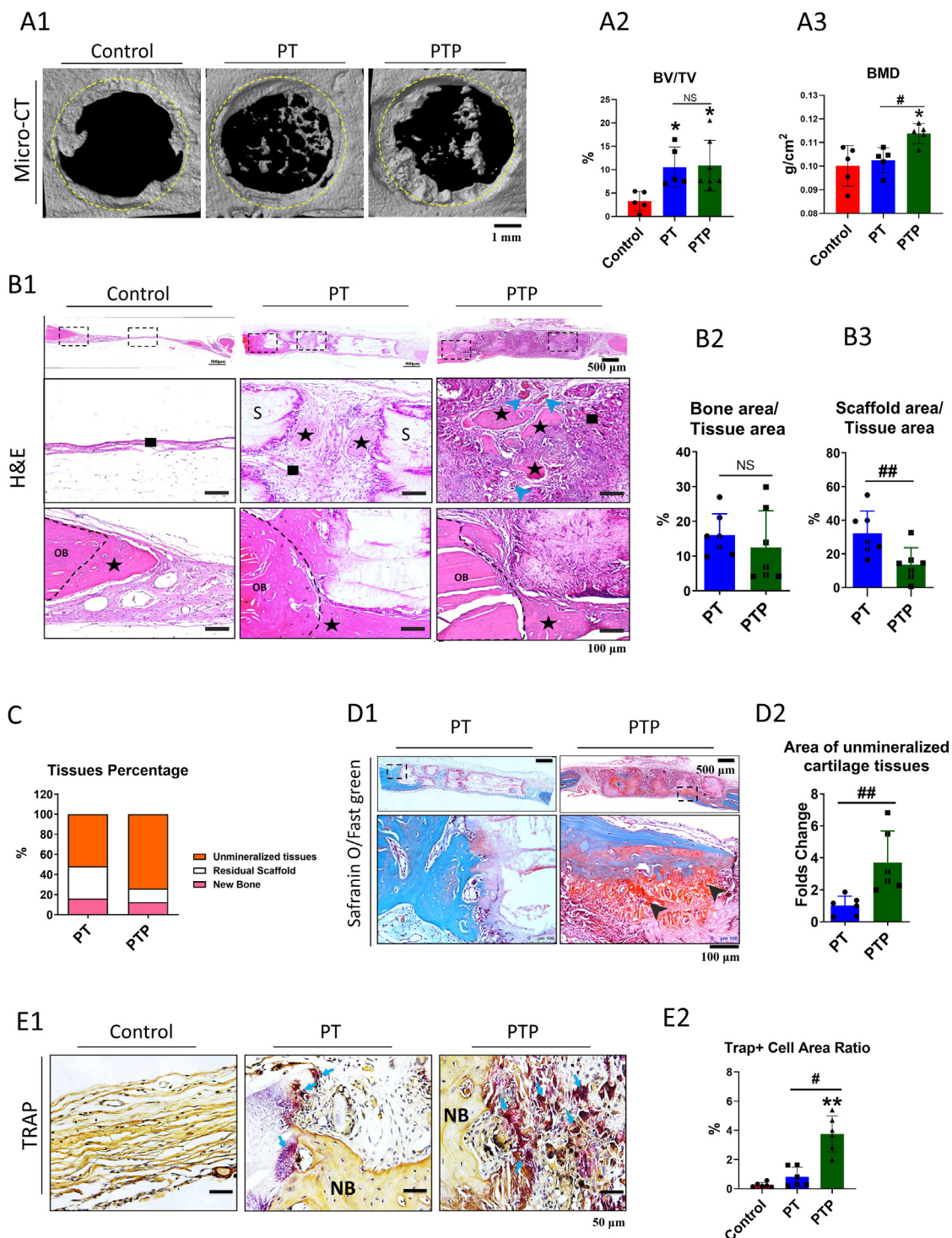
Fig. 4. New bone formation within defect regions after 8 weeks of implantation. A1: Micro-CT images of newly formed bone within bone defect regions at 8 weeks post-operation. Margins of original defect are indicated by dashed yellow lines, bar = 1 mm. A2: Bone volume/tissue volume (BV/TV, %) within bone defect region 5 mm in diameter at 8 weeks was detected by micro-CT, n = 5. A3: Bone mineral density in the rat calvarial defect area measured with DXA at 8 weeks of implantation, n = 5. B1: Histological sections of H&E staining post-implantation for 8 weeks, bar = 500 μm. The newly formed bone was marked by ★; Fibrous tissues were marked by ■; Blue arrows showed the new vessels; "S" meant the residual scaffold, bar = 100 μm. B2-3: Quantification of newly formed bone, scaffold remains in the defect regions, n = 7. ##$p < 0.01$. B2-3: Tissue area percentage analysis of newly formed bone, scaffold remains, other tissues in the defect regions, n = 7. *$p < 0.05$, **$p < 0.01$, when compared to the Control group; #$p < 0.05$, ##$p < 0.01$, when compared between PT and PTP groups. C: Tissue area percentage analysis of newly formed bone, scaffold remains, unmineralized tissues in the defect regions, n = 7. D1: Histological sections of Safranin O red/Fast green Staining at 8 weeks. The color orange represented the stain of unmineralized cartilage tissue, while the green/blue represented bone tissue, bar = 500 μm. The black arrows pointed to unmineralized cartilage tissue, bar = 100 μm. D2: Quantification of unmineralized cartilage tissue in the defect treated with PT and PTP scaffold at 8 weeks E: Histological sections of TRAP staining post-implantation for 8 weeks in PT and PTP group, bar = 50 μm. E1: The "NB" meant the newly formed bone tissue and the blue arrow showed osteoclast which was red by TRAP kit staining. E2: Quantification of the ratio of TRAP + cells area in the defect sites treated with PT and PTP scaffold at 8 weeks. n = 6. *$p < 0.05$, **$p < 0.01$, when compared to the Control group; #$p < 0.05$, ##$p < 0.01$, when compared between PT and PTP groups.
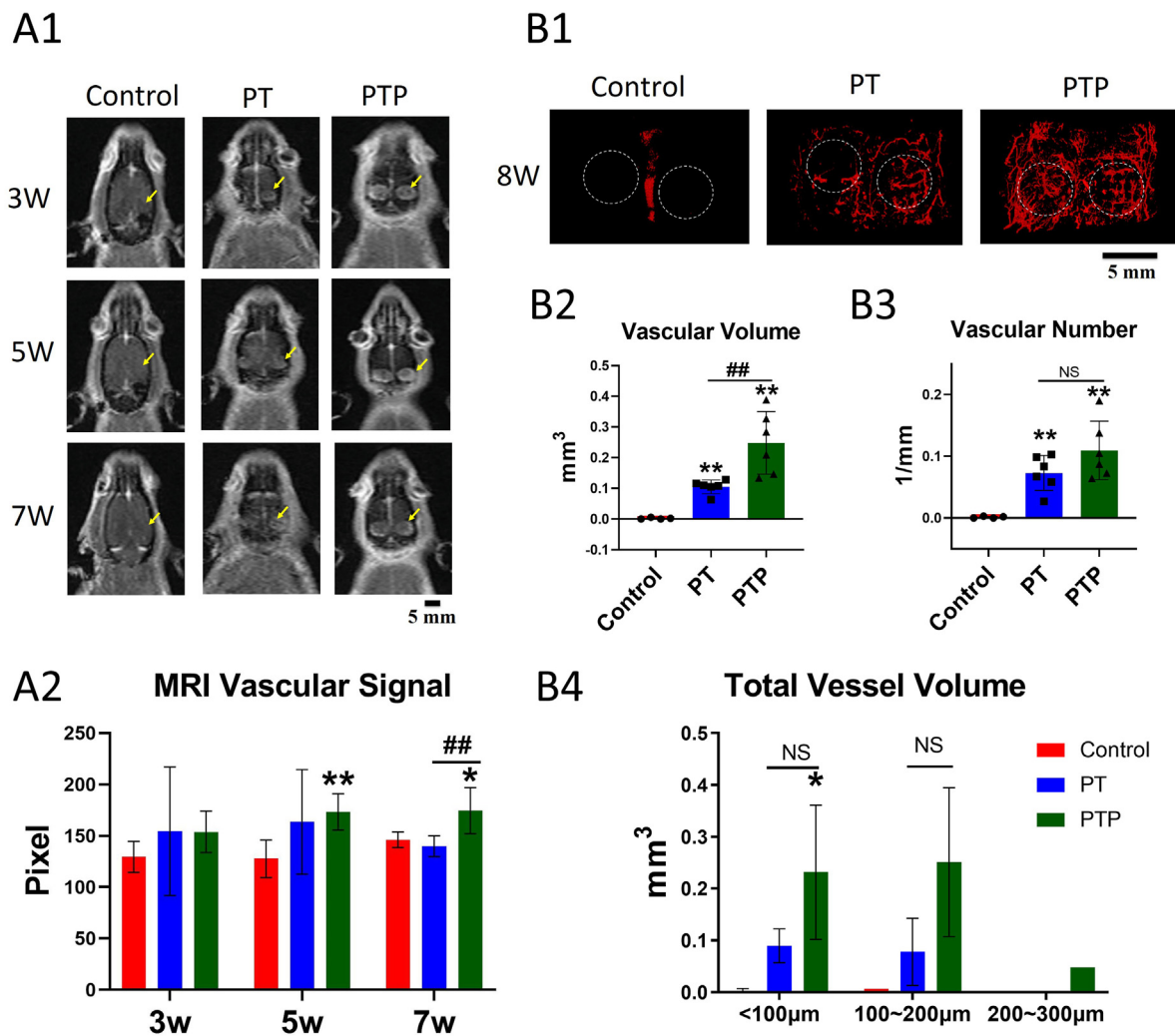
Fig. 5. New vessel formation within defect regions after 8 weeks of implantation. A: Representative DCE-MRI images were acquired in the cranial bone of rats when the signal intensity (SI) continuously increased until reaching the initial maximum enhancement after 3, 5, and 7 weeks post-implantation (A1), bar = 5 mm. The average IOD of SI within implantation regions (A2), n = 6. B: 3D reconstructed images of micro-CT-based angiography in the cranial bone at 8 weeks post-implantation. The region of interest (ROI) was chosen (the white circle) along with the periphery of the defect region (B1), bar = 5 mm, the quantitative statistic of the vascular volume (B2) and vascular number (B3), and the distribution of vessels with difference volume (B4). Small-sized ($<$100 μm), medium-sized (100–200 μm), large-sized ($>$200 μm). n = 3. *$p < 0.05$, **$p < 0.001$, when compared to the Control group; #$p < 0.05$, ##$p < 0.01$, when compared between PT and PTP groups.

= 0.0003) and the PT groups ($p = 0.001$) (Fig. 6C). These findings suggested that the PTP scaffold could synergistically promote neovascularization and bone formation within the rat calvarial defect region. This study also found CD31 marked newly formed vessels were increased within PTP implantation regions than that of the PT group (Fig. S9).

4. Discussion

In this study, we successfully developed a PTP scaffold as a potential orthopedical implant, which could promote the repair of critical-size bone defects through the slow release of a safety and efficacy puerarin concentration for facilitating angiogenesis and osteogenesis. First yet highlight, we identified that puerarin indirectly facilitated angiogenesis of endothelial cells by increasing VEGF expression of osteoblasts.

Our previously established PLGA/TCP (the mass ratio of PLGA to TCP was 4:1) scaffold with 400–500 μm pore size and 60–80% porosity, which exhibited good biocompatibility, osteoconductivity, and biodegradability *in vitro* and *in vivo*, and we spent the last decade attempt to a bench-to-bed translation of PLGA/TCP-based composite [12–14]. China also was encouraging the development of innovative medical products.

From 2014 to 2018, the NMPA set up a special approval path for innovative medical devices and also issued the medical device priority approval procedure for special medical devices [17]. Under the policies' promotion, we have developed a PLGA/TCP/Mg (PT-Mg) scaffold as a non-weight-bearing combination orthopedic device and have been approved to conduct clinical trials in China. Because Mg is not a drug, thus Mg does not be required to have a drug registration certificate issued by NMPA. Puerarin is a long-term clinical use drug as an adjuvant treatment of coronary heart disease and myocardial infarction [20]. Recently, puerarin was reported to have the ability to regulate bone metabolism and promote osteogenesis [22,34,35]. Thus, we selected the PT scaffold as a carrier for puerarin and aim to present a potential drug/medicine combination implant. As expected, puerarin incorporation into PT scaffold inherited all advantages of PT scaffold *in vitro*, without changing the structural, mechanical, and biodegradation properties of PT scaffold.

Drug/device combination implant that enhanced functions by releasing drugs to the intended site, and the additional drugs may bring new benefits as well as risks. Thus, *in vitro* release study could be used to evaluate the stability and safety of the final implant, and conduct the
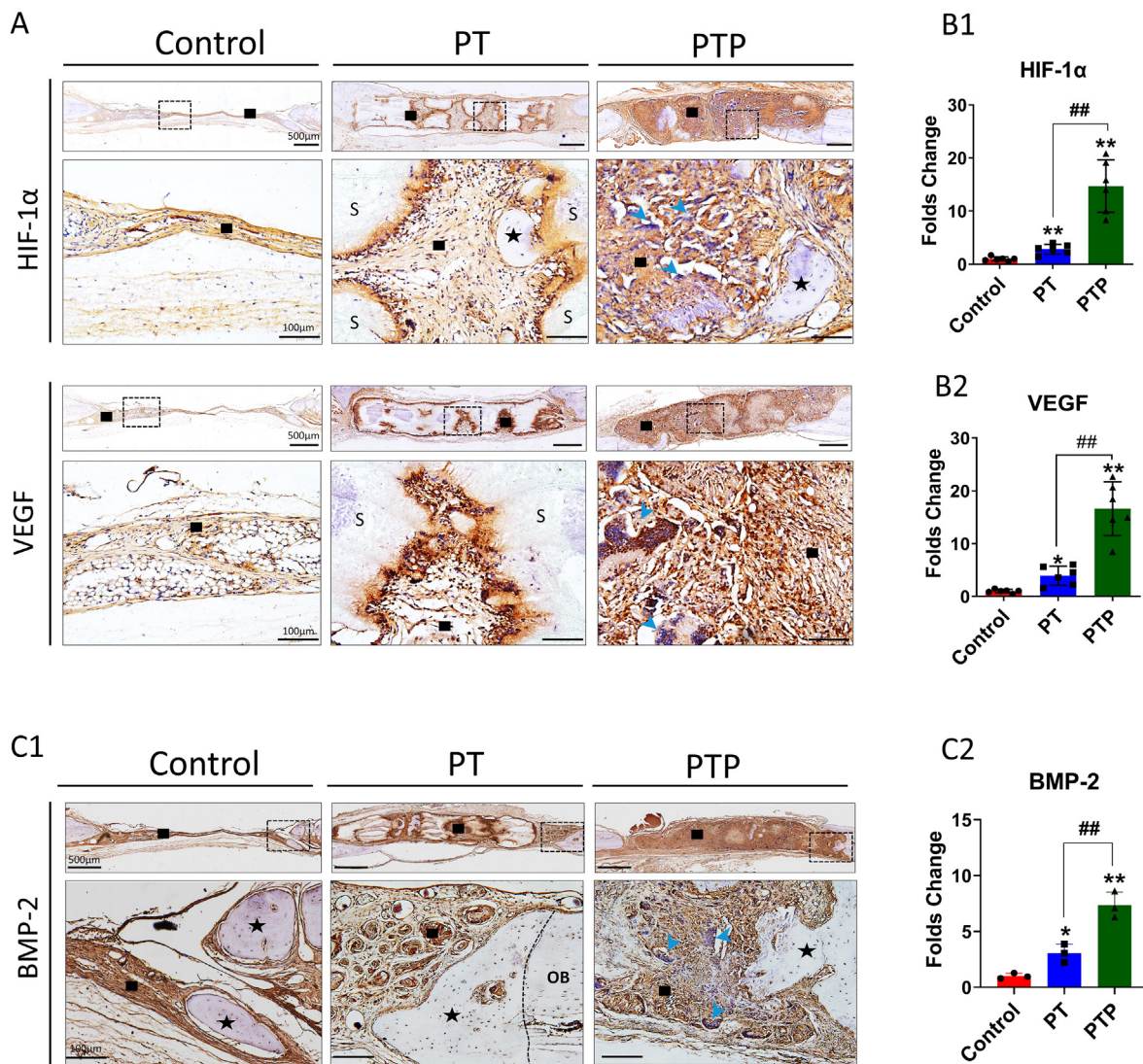
Fig. 6. Immunohistochemical staining analysis within the calvarial defect. A: HIF-1α and VEGF expression levels were detected by immunohistochemical analysis, bar = 500 μm. The newly formed bone was marked by ★; The positive stained brown tissue ■; Blue arrows showed the multinuclear cells; "S" meant the residual scaffold, bar = 100 μm. Quantitative analysis of HIF-1α (B1), and VEGF (B2) was assessed using Image-Pro Plus software with a dedicated imaging analysis software, n=6. **$p < 0.01$, when compared to the Control group; ##$p < 0.01$, when compared between PT and PTP groups. C1: BMP-2 expression level was detected by immunohistochemical analysis, bar=500 μm. The newly formed bone was marked by ★; The positive stained brown tissue was marked by ■; Blue arrows showed the multinuclear cells; "OB" meant the older bone tissue, bar=100 μm. C2: Quantitative analysis of BMP-2, n=3.

qualitative and quantitative investigation of the combination device in the process of registration test [17]. In this study, puerarin releasing from the PTP scaffold was stable and continuous with a constant speed and lasted for more than 5 months. We found that puerarin loading by LT-RP technology did not change the biodegradation characteristics of PT. The pH value of the degradation medium, as well as the accumulated Ca2+ ions concentration among those PT and PTP scaffolds, were similar. However, drug release from scaffold was varying the drug loading method and materials combination [36]. The drug was directly loaded onto the calcium phosphate cement (CPC) matrix, the drug release rates increased with the total porosity of the matrix, as well as the bulk of the CPC [37]. When the drug was encapsulated into a biodegradable PLGA firstly, then subsequently incorporated into the CPC matrix, showed a prolonged release, the release rates affected by the polymer degradation, and a decreased burst release for all the formulations as compared to those involving the direct drug loading onto CPC [38]. In the present study, the puerarin was directly loaded on the mixture matrix of β-TCP

and PLGA, thus the puerarin released from the implant was slowly and continuously. The drug release rate was governed by the PLGA relaxation and also by the subsequent drug diffusion from within the bulk of the β-TCP. When the polymer underwent degradation, the second stage or the third stage of sustained drug release takes place. Meanwhile, the solubility test indicated that puerarin possessed positive Gibbs free energies in water solution, and puerarin preferred to dissolve in acid nonpolar solvents [39]. Thus, in physiological fluids the dissolved dosage of puerarin was safe. Biosafety analysis *in vitro* showed that the PTP scaffold offered a favorable surface property and micro-environment for mediating endothelial cell creeping and ingrowth. Consistently, the degradation medium of the PTP scaffold also promoted osteoblastic-like cell proliferation.

During the degradation process, the PTP scaffold's architecture showed more stability and maintained its porous structure and shape for at least 10 weeks without deformations and cracks. The pH value of the degraded medium maintained at 7.0–7.5 before 10 weeks, then declined and reached

the lowest value (pH = 4.5) at 150 days post-degradation. Biomaterial degradation *in vitro* is different from biodegradation *in vivo*. The degradation of the scaffolds *in vitro* was under a simple condition, and the decreased pH value resulted from the formation of the acidic degradation products [40,41]. The harmful effect of the acidic degradation products would be reduced *in vivo* due to circulating body fluid and finally hydrolyzed into water and carbon dioxide in the body [42]. In addition, our results showed approximately 68% of the PT and 86% of the PTP scaffolds had been degraded at 8 weeks post-implantation.

In the present study, the potency of the PTP scaffold as a non-weight-bearing bone graft was analyzed and has successfully demonstrated that PTP scaffold implantation led to structural and functional bone regeneration in a critical-size bone defect model in rats. On implantation of a scaffold into a bone defect site, the implant as a template should offer optimal biomechanical conditions and geometrical shapes for mediating cell in-growth and vascularization. Importantly, this scaffold also should stimulate and support the continuance of bone in-growth as well as subsequent remodeling and maturation [2]. In the present study, the PTP scaffold was implanted for 8 weeks, there was notable mineralized bone formation around the PTP scaffold struts. We also observed enhanced bone bridging within defect sites as the scaffold gradually degraded. Although the BV/TV (%) within defect sites showed no difference between PT and PTP groups, the BMD of newly formed bone was significantly higher in the PTP group, which indicated the regenerated bone tissue within the scaffold has been remodeled. This paradigm shift was particularly relevant to structural and functional bone formation [43].

Sufficient vascularity was necessary for a valid bone repair [6]. Microfil angiography was performed to determine the vessel volume and number and demonstrated there was sufficient vascularization throughout the entire scaffold, and the bone reconstruction of defect sites could be directed by the newly formed vessels pattern within the scaffold [44]. The newly formed vessels within the defect site presented well-architecture, and the vascular perfusion capacity was gradually reconstructed as the vessel's network. At 8 weeks, PTP scaffold architecture was still evident after implantation. Histological observation found the pores were filled with unmineralized repair tissue and vascularity. There was the enhancing CD31 marked vessels formation within the repair regions where the PTP scaffold degraded, and they would recruit mesenchymal progenitor cells for bone regeneration [45]. Consistently, higher HIF-α, VEGF and BMP-2 expression levels in those regenerated tissue further indicated high remodeling activity, and those unmineralized cartilage tissues usually meant immature bone.

To explore the mechanism of the PTP scaffold in promoting valid bone repair, we designed and executed an *in vitro* study, and have found that stable released puerarin from the PTP scaffold could mediate the interaction of the surrounding cells, and then puerarin would combine with the succeeding Ca^{2+} ions released from the PTP scaffold to participate into the subsequent repair events. Our results showed the degradation medium with active substances released from the PTP scaffold also could accelerate osteoblastic differentiation, maturation, and calcium nodules formation of MC3T3-E1 cells. The study demonstrated that puerarin could regulate intracellular and extracellular Ca^{2+} ions concentrations of MC3T3-E1 cells through mediating nonselective cation channel TRPM3 activated status to facilitate osteoblastic differentiation and mineralization [46]. Thus, the stable and continuous puerarin releasing endowed the PT scaffold with excellent osteogenic ability. Although *in vitro* results showed the degradation medium of the PTP scaffold did not affect tube-like structure formation of EA. hy 926 cells directly, when PTP scaffold degradation cultured MC3T3-E1 cells first, then collected this conditional medium to stimulate EA. hy 926 cells, the stimulated endothelial cells would prefer to form tube-like structure in matrigel. Further study demonstrated that puerarin-enriched degradation medium could promote MC3T3-E1 cells expressing VEGF and BMP-2, enhancing angiogenesis and osteogenesis. Thus, we considered that puerarin could regulate the local bone repair microenvironment by increasing VEGF and BMP-2 levels to conduct the interaction of the surrounding cells, subsequently induced vascular infiltration, recruited repair cells, and conducted downstream repair events progressing in a well-organized pattern [8].

However, the regenerated tissue with sufficiency vascularity as "younger bone" was more within defect sites in the PTP group than that in the PT group, and no inflammation was found in the surgery area in all groups throughout the animal experiment. We have observed a lot of TRAP + cells were found in the regenerated tissue in the PTP group. Some studies found that the TRAP + osteoclasts cells and macrophages cells directly took part in cell-mediated calcium phosphate-based biomaterials resorption in the bone tissue [47]. In addition, we observed that the residual materials in the PTP group were less than those in the PT group, and the newly formed tissues gradually replaced the degrading PTP scaffold. Thereby, the biodegradation of the PTP scaffold might be relative to the elevated TRAP + cells *in vivo* [47,48]. In addition, the enhanced BMD of newly formed bone in the PTP group further indicated the remodeling program started with TRAP + osteoclasts formation.

The relationship between scaffold degradation and bone tissue regeneration *in vivo* was complex. Although the interaction between PTP scaffold degradation and new tissue in-growth and maturation is difficult to be accurately described in animal experiments, it is indispensable for evaluating the efficacy and safety of drug/device combination medical implant before clinical translation. One limitation in the present study is that we do not explore the direct effect of real-time released puerarin on cells during PTP scaffold degradation. The degradation property of PTP scaffold *in vivo* and the interaction between degradation scaffold and newly formed tissue will be investigated in the future.

5. Conclusion

The developed PTP scaffold with stable puerarin release presented good biocompatibility and osteoconductivity both *in vitro* and *in vivo*. It demonstrated good structural and functional bone formation for accelerating critical-sized bone defect repair. Mechanism study revealed that the PTP scaffold could stimulate peri-implant tissues secreting VEGF and BMP-2 to achieve angiogenesis coupling with osteogenesis. The PTP scaffold presents a potential drug/device combination medical implant for large bone defect repair, which also provides a new and innovative application for the 'old drug' puerarin.

Authorship

Conception and design of the study: Xinluan Wang, Ling Qin, Yongbo Gao; Acquisition of data: Huijuan Cao, Lingli Li, Ling Li, Xiangbo Meng, Yanzhi Liu, Wenxiang Cheng; Analysis and/or interpretation of data: Huijuan Cao, Lingli Li, Ling Li, Xiangbo Meng; Drafting the manuscript: Huijuan Cao, Lingli Li, Ling Li, Xinluan Wang; Revising the manuscript critically for important intellectual content: Xinluan Wang; Ling Qin, Peng Zhang, Yongbo Gao; Approval of the version of the manuscript to be published (the names of all authors must be listed): Huijuan Cao, Lingli Li, Ling Li, Xiangbo Meng, Yanzhi Liu, Wenxiang Cheng, Peng Zhang, Yongbo Gao, Ling Qin, Xinluan Wang.

Declaration of competing interest

There is no conflict of interest to declare.

Acknowledgment

Appendix A. Supplementary data

Supplementary data to this article can be found online at https://doi.org/10.1016/j.jot.2022.05.003.

References

[1] Carano RA, Filvaroff EH. Angiogenesis and bone repair. Drug Discov Today 2003; 8(21):980–9.

[2] Koons GL, Diba M, Mikos AG. Materials design for bone-tissue engineering. Nat Rev Mater 2020;5(8):584–603.

[3] Schemitsch EH. Size matters: defining critical in bone defect size. J Orthop Trauma 2017;31:S20–2.

[4] Gibon E, Lu LY, Nathan K, Goodman SB. Inflammation, ageing, and bone regeneration. J Orthop Translat 2017;10:28–35.

[5] Eming SA, Wynn TA, Martin P. Inflammation and metabolism in tissue repair and regeneration. Science 2017;356(6342):1026–30.

[6] Hankenson KD, Dishowitz M, Gray C, Schenker M. Angiogenesis in bone regeneration. Injury 2011;42(6):556–61.

[7] Saran U, Gemini Piperni S, Chatterjee S. Role of angiogenesis in bone repair. Arch Biochem Biophys 2014;561:109–17.

[8] Patel ZS, Young S, Tabata Y, Jansen JA, Wong ME, Mikos AG. Dual delivery of an angiogenic and an osteogenic growth factor for bone regeneration in a critical size defect model. Bone 2008;43(5):931–40.

[9] Devescovi V, Leonardi E, Ciapetti G, Cenni E. Growth factors in bone repair. Chir Organi Mov 2008;92(3):161–8.

[10] Kang F, Yi Q, Gu P, Dong Y, Zhang Z, Zhang L, et al. Controlled growth factor delivery system with osteogenic-angiogenic coupling effect for bone regeneration. J Orthop Translat 2021;31:110–25.

[11] Gaharwar AK, Singh I, Khademhosseini A. Engineered biomaterials for in situ tissue regeneration. Nat Rev Mater 2020;5(9):686–705.

[12] Xie XH, Wang XL, Zhang G, He YX, Leng Y, Tang TT, et al. Biofabrication of a PLGA-TCP-based porous bioactive bone substitute with sustained release of icaritin. J Tissue Eng Regen Med 2015;9(8):961–72.

[13] Lai YX, Cao HJ, Wang XL, Chen SK, Zhang M, Wang N, et al. Porous composite scaffold incorporating osteogenic phytomolecule icariin for promoting skeletal regeneration in challenging osteonecrotic bone in rabbits. Biomaterials 2018;153: 1–13.

[14] Lai YX, Li Y, Cao HJ, Long J, Wang XL, Li L, et al. Osteogenic magnesium incorporated into PLGA/TCP porous scaffold by 3D printing for repairing challenging bone defect. Biomaterials 2019;197:207–19.

[15] Shi GS, Li YY, Luo YP, Jin JF, Sun YX, Zheng LZ, et al. Bioactive PLGA/tricalcium phosphate scaffolds incorporating phytomolecule icaritin developed for calvarial defect repair in rat model. J Orthop Translat 2020;24:112–20.

[16] Cheng WX, Liu YZ, Meng XB, Zheng ZT, Li LL, Ke LQ, et al. PLGA/beta-TCP composite scaffold incorporating cucurbitacin B promotes bone regeneration by inducing angiogenesis. J Orthop Translat 2021;31:41–51.

[17] Tian J, Song X, Wang Y, Cheng M, Lu S, Xu W, et al. Regulatory perspectives of combination products. Bioact Mater 2021.

[18] Yang C, Li J, Zhu K, Yuan X, Cheng T, Qian Y, et al. Puerarin exerts protective effects on wear particle-induced inflammatory osteolysis. Front Pharmacol 2019; 10(1113).

[19] Ai F, Chen M, Yu B, Yang Y, Xu G, Gui F, et al. Puerarin accelerate scardiac angiogenesis and improves cardiac function of myocardial infarction by upregulating VEGFA, Ang-1 and Ang-2 in rats. Int J Clin Exp Med 2015;8(11): 20821–8.

[20] Zhou YX, Zhang H, Peng C. Puerarin: a review of pharmacological effects. Phytother Res 2014;28(7):961–75.

[21] Liu H, Li W, Ge X, Jia S, Li B. Coadministration of puerarin (low dose) and zinc attenuates bone loss and suppresses bone marrow adiposity in ovariectomized rats. Life Sci 2016;166:20–6.

[22] Wang N, Wang X, Cheng W, Cao H, Zhang P, Qin L. Puerarin promotes osteogenesis and inhibits adipogenesis in vitro. Chin Med 2013;8(1):1749–8546.

[23] Qiu Z, Li L, Huang Y, Shi K, Zhang L, Huang C, et al. Puerarin specifically disrupts osteoclast activation via blocking integrin-beta3 Pyk2/Src/Cbl signaling pathway. J Orthop Translat 2022;33:55–69.

[24] Turer CC, Turer A, Durmuslar MC, Onger ME. The local effect of puerarin on critical-sized calvarial defects. J Craniofac Surg 2017;28(1):143–6.

[25] Wong R, Rabie B. Effect of puerarin on bone formation. Osteoarthritis Cartilage 2007;15(8):894–9.

[26] Xie XH, Wang XL, Zhang G, He YX, Wang XH, Liu Z, et al. Structural and degradation characteristics of an innovative porous PLGA/TCP scaffold incorporated with bioactive molecular icaritin. Biomed Mater 2010;5(5):054109.

[27] Li L, Long J, Cao H, Tang T, Xi X, Qin L, et al. Quantitative determination of residual 1,4-dioxane in three-dimensional printed bone scaffold. J Orthop Translat 2017;13: 58–67.

[28] Chen SH, Wang XL, Xie XH, Zheng LZ, Yao D, Wang DP, et al. Comparative study of osteogenic potential of a composite scaffold incorporating either endogenous bone morphogenetic protein-2 or exogenous phytomolecule icaritin: an in vitro efficacy study. Acta Biomater 2012;8(8):3128–37.

[29] Li C, Sun J, Shi K, Long J, Li L, Lai Y, et al. Preparation and evaluation of osteogenic nano-MgO/PMMA bone cement for bone healing in a rat critical size calvarial defect. J Mater Chem B 2020;8(21):4575–86.

[30] Spicer PP, Kretlow JD, Young S, Jansen JA, Kasper FK, Mikos AG. Evaluation of bone regeneration using the rat critical size calvarial defect. Nat Protoc 2012;7(10): 1918–29.

[31] Mistry AS, Pham QP, Schouten C, Yeh T, Christenson EM, Mikos AG, et al. In vivo bone biocompatibility and degradation of porous fumarate-based polymer/ alumoxane nanocomposites for bone tissue engineering. J Biomed Mater Res 2010; 92(2):451–62.

[32] Nettleton K, Luong D, Kleinfehn AP, Savariau L, Premanandan C, Becker ML. Molecular mass-dependent resorption and bone regeneration of 3D printed PPF scaffolds in a critical-sized rat cranial defect model. Adv Healthc Mater 2019;8(17): e1900646.

[33] Yu W, Li R, Long J, Chen P, Hou A, Li L, et al. Use of a three-dimensional printed polylactide-coglycolide/tricalcium phosphate composite scaffold incorporating magnesium powder to enhance bone defect repair in rabbits. J Orthop Translat 2019;16:62–70.

[34] Wang C, Meng M-X, Tang X-L, Chen K-M, Zhang L, Liu W-N, et al. The proliferation, differentiation, and mineralization effects of puerarin on osteoblasts in vitro. Chin J Nat Med 2014;12(6):436–42.

[35] Park KH, Gu DR, Jin SH, Yoon CS, Ko W, Kim YC, et al. Pueraria lobate inhibits RANKL-mediated osteoclastogenesis via downregulation of CREB/PGC1β/c-Fos/ NFATc1 signaling. Am J Chin Med 2017;45(8):1725–44.

[36] Fosca M, Rau JV, Uskokovic V. Factors influencing the drug release from calcium phosphate cements. Bioact Mater 2022;7:341–63.

[37] Hofmann MP, Mohammed AR, Perrie Y, Gbureck U, Barralet JE. High-strength resorbable brushite bone cement with controlled drug-releasing capabilities. Acta Biomater 2009;5(1):43–9.

[38] Schnieders J, Gbureck U, Vorndran E, Schossig M, Kissel T. The effect of porosity on drug release kinetics from vancomycin microsphere/calcium phosphate cement composites. J Biomed Mater Res B Appl Biomater 2011;99(2):391–8.

[39] Wei D, Zhang X. Solubility of puerarin in the binary system of methanol and acetic acid solvent mixtures. Fluid Phase Equil 2013;339:67–71.

[40] Makadia HK, Siegel SJ. Poly lactic-co-glycolic acid (PLGA) as biodegradable controlled drug delivery carrier. Polymers 2011;3(3):1377–97.

[41] Kim MS, Ahn HH, Yu NS, Mi HC, Khang G, Hai BL. An in vivo study of the host tissue response to subcutaneous implantation of PLGA- and/or porcine small intestinal submucosa-based scaffolds. Biomaterials 2007;28(34):5137–43.

[42] Kapoor DN, Bhatia A, Kaur R, Sharma R, Kaur G, Dhawan S. PLGA: a unique polymer for drug delivery. Ther Deliv 2015;6(1):41–58.

[43] Woodruff MA, Lange C, Reichert J, Berner A, Chen FL, Fratzl P, et al. Bone tissue engineering: from bench to bedside. Mater Today 2012;15(10):430–5.

[44] Liu WC, Chen S, Zheng L, Qin L. Angiogenesis assays for the evaluation of angiogenic properties of orthopaedic biomaterials - a general review. Adv Healthc Mater 2017;6(5).

[45] Kusumbe AP, Ramasamy SK, Adams RH. Coupling of angiogenesis and osteogenesis by a specific vessel subtype in bone. Nature 2014;507(7492):323–8.

[46] Zeng X, Feng Q, Zhao F, Sun C, Zhou T, Yang J, et al. Puerarin inhibits TRPM3/miR-204 to promote MC3T3-E1 cells proliferation, differentiation and mineralization. Phytother Res 2018;32(6):996–1003.

[47] Sheikh Z, Abdallah MN, Hanafi AA, Misbahuddin S, Rashid H, Glogauer M. Mechanisms of in vivo degradation and resorption of calcium phosphate based biomaterials. Materials 2015;8(11):7913–25.

[48] Gao C, Peng S, Feng P, Shuai C. Bone biomaterials and interactions with stem cells. Bone Res 2017;5:17059.